Journal of Hazardous Materials 192 (2011) 1683–1689

Contents lists available at ScienceDirect

Journal of Hazardous Materials

journal homepage: www.elsevier.com/locate/jhazmat

Anodic oxidation of wastewater containing the Reactive Orange 16 Dye using heavily boron-doped diamond electrodes

F.L. Migliorini[a], N.A. Braga[b], S.A. Alves[c], M.R.V. Lanza[c], M.R. Baldan[a], N.G. Ferreira[a,*]

[a] Instituto Nacional de Pesquisas Espaciais, INPE, 12245-970, São José dos Campos, SP, Brazil
[b] Departamento de Química, Instituto de Ciências Exatas, Universidade Federal do Amazonas, UFAM, 69077-000, Manaus, Am, Brazil
[c] Instituto de Química de São Carlos, Universidade de São Paulo, 13560-970, São Carlos, SP, Brazil

ARTICLE INFO

Article history:
Received 11 February 2011
Received in revised form 31 May 2011
Accepted 1 July 2011
Available online 18 July 2011

Keywords:
BDD electrode
Azo-dye
Advanced oxidation process
Wastewater

ABSTRACT

Boron-doped diamond (BDD) films grown on the titanium substrate were used to study the electrochemical degradation of Reactive Orange (RO) 16 Dye. The films were produced by hot filament chemical vapor deposition (HFCVD) technique using two different boron concentrations. The growth parameters were controlled to obtain heavily doped diamond films. They were named as E1 and E2 electrodes, with acceptor concentrations of 4.0 and 8.0×10^{21} atoms cm^{-3}, respectively. The boron levels were evaluated from Mott–Schottky plots also corroborated by Raman's spectra, which characterized the film quality as well as its physical property. Scanning Electron Microscopy showed well-defined microcrystalline grain morphologies with crystal orientation mixtures of (1 1 1) and (1 0 0). The electrode efficiencies were studied from the advanced oxidation process (AOP) to degrade electrochemically the Reactive Orange 16 azo-dye (RO16). The results were analyzed by UV/VIS spectroscopy, total organic carbon (TOC) and high-performance liquid chromatography (HPLC) techniques. From UV/VIS spectra the highest doped electrode (E2) showed the best efficiency for both, the aromaticity reduction and the azo group fracture. These tendencies were confirmed by the TOC and chromatographic measurements. Besides, the results showed a direct relationship among the BDD morphology, physical property, and its performance during the degradation process.

1. Introduction

The textile wastewaters have characteristics such as strong color, large numbers of suspended solids, broadly fluctuating pH, high chemical oxygen demand (COD), and biological toxicity. All these characteristics contribute to turn this kind of effluent an environmental problem in our days. Most of these problems are due to the nature of the organic molecules that compose the dyes present in textile wastewaters. In this context, azo-dyes form a large group of organic molecules and represent the largest class of dyes used in textile processing and other industries [1–3]. Their molecules are formed from a system of aromatic moieties linked by chromophobic azo groups (–N=N–) in association with auxochromes as –OH, $–SO_3$ groups.

The complexity of the azo-dye molecules turns the conventional methods unsatisfactory for wastewater treatment. The need to investigate new alternatives for the adequate treatment of azo-dye wastewaters is related to their carcinogenic or mutagenic character, deleterious effect of the color in the receiving waters, and customary resistance of the effluents to biological degradation [3].

Considering that the dyes present high stability under sunlight and resistance to microbial attack and temperature, in general, these compounds are not degradable in conventional wastewater treatment plants. In this sense, Martínez-Huille and Brillas [4] have described in an extensive way the main technologies utilized for the removal of these pollutants. The technologies for dye removal from wastewaters are classified as: physico-chemical methods [5–7], chemical methods [5,6,8,9], advanced oxidation processes (AOPs) [5,6,8,9], microbiological treatments [5–7], enzymatic decomposition [5], and electrochemical methods [8,10–18]. So, considering many works presented in the literature we will summarize a comparison of the various characteristics of such technologies in Table 1.

According to Table 1, one alternative process refers to chemical treatment procedure that removes organic and inorganic materials by oxidation. Specifically, the Advanced Oxidation Processes (AOP) are clean and are able to decompose a great number of compounds with selectivity [4,19–22]. These processes are characterized by the transformation of a large number of organic pollutants into carbon dioxide, water and inorganic anions through degradation reactions involving oxidative transitory species, mainly the hydroxyl radical

* Corresponding author. Tel.: +55 12 3208 6675; fax: +55 12 3208 6717.
E-mail address: neidenei@las.inpe.br (N.G. Ferreira).

0304-3894/$ – see front matter © 2011 Elsevier B.V. All rights reserved.
doi:10.1016/j.jhazmat.2011.07.007

Table 1
Comparison among the main methods for the removal of organic dyes from wastewaters.

Methods	Advantages/disadvantages	Refs
Physico-chemical	Effective discoloration/restricted application by the formation of sludge	[5–7]
Chemical	Fast discoloration/expensive and have operation problems	[5,6,8,9]
AOPs	Fast discoloration/expensive and have operation problems	[5,6,8,9]
Microbiological	Attractive and simple/very inefficient, dye compounds are resistant to microbiological attack	[5–7]
Enzymatic decomposition	Requires a greater knowledge of the enzymatic process for application	[5]
Electrochemical methods	Environmental compatibility due to use a clean reagent, the electron.	[8,10–18]

(•OH). AOP has been demonstrated to produce hydroxyl radicals electrochemically in an anodic reaction directly from the water [23]. These hydroxyl radicals react strongly with all organic substances usually by hydrogen abstraction.

Besides to its environmental compatibility, the electrochemical process presents important advantages related to its versatility, high energy efficiency, amenability of automation and safety because it operates at mild conditions [10,14,17]. Electrochemical oxidation with different anodes and indirect electro-oxidation with active chlorine are typical methods for the removal of dye pollutants. It is classified as electrochemical advanced oxidation process (EAPO) and consists in the oxidation of pollutants in an electrolytic cell by chemical reaction with electrogenerated species from water discharge at the anode.

By using the electrochemical production of hydroxyl radicals the boron-doped diamond (BDD) thin film seems to be a suitable electrode material. The BDD based anode is a new electrode material which has received great attention in the field of wastewater treatment for its wide potential window, low background current, very low activity for O_2 evolution reaction and high anodic potential [24]. Another advantage to use BDD electrodes for organic degradation is related to its inertness, which forbids some undesirable by-products or products to strongly adsorb on BDD surface. In most of the cases, it is just necessary to rinse BDD surface with an appropriate solvent to remove the adsorbed species. This problem is solved by applying high anodic or cathodic potentials for problematic surface passivators such as: chlorophenols [25], nitrophenol, and aromatic amine [26,27] potentials.

BDD electrode is considered as a "non-active" anode. In general, the accepted reactions for the mechanism involved in the mineralization of organic pollutants (R) on BDD, at the anode active sites (M) and in aqueous solutions, propose the production of adsorbed hydroxyl radicals (M(•OH)ads) at the BDD anode surface which is directly responsible for the generation of the mineralization products (MP):

$$R(aq) + (n/2)M(\bullet OH)ads \rightarrow (n/2)M + MP + (n/2)H^+ + (n/2)e^- \quad (1)$$

$$M(\bullet OH)ads \rightarrow M + (1/2)O_2 + H^+ + e^- \quad (2)$$

where n is the number of electrons involved in the organic oxidation reactions. Reaction (1) is in competition with reaction (2) which is correlated with the anodic discharge of •OH radicals generating oxygen gas. The number of electrogenerated •OH radicals are strongly associated to their interaction with the anode surface [28]. The electrogenerated •OH radicals formed on the BDD from the water oxidation molecules lead to the formation of physisorbed hydroxyl. The anode surface interaction with the •OH is so weak that allows the direct reaction of organics with M(•OH) resulting in the mineralization of organic compounds. So, a non-active electrode does not participate in the direct anode reaction of organics and does not provide any catalytic active site for their adsorption from the aqueous media.

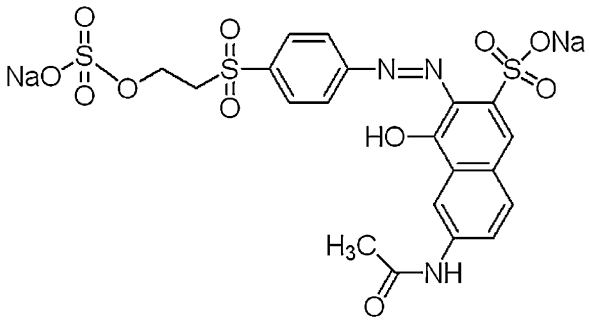

Fig. 1. Structural formula of the Reactive Orange 16 (RO16) azo-dye.

Otherwise, comparing to other electrodes, so-called "active" anodes, such as Pt, IrO_2, and RuO_2, for the initial reaction as in both kind of anodes to form (M(•OH), the surface of active anodes interacts strongly with (•OH). Then, a so called higher oxide or superoxide (MO) may be formed. This may occur when higher oxidation states are available for a metal oxide anode, above the standard potential for oxygen evolution ($E^0 = 1.23$ vs. SHE). The redox couple MO/M acts as a mediator in the oxidation of organics, which competes with the reaction of oxygen evolution via chemical decomposition of the higher oxide species [4].

In this work, EAOP performed from BDD based anodes with different boron concentrations, named E1 and E2, was used to study the Reactive Orange 16 dye (RO16) degradation. The structural formula of the main molecule present in this textile azo-dye is shown in Fig. 1. This dye was chosen because it is biological refractory and resistant to the degradation. The concentration of the RO16 azo-dye was monitored by analytical techniques in order to understand the RO16 degradation process. The RO16 azo-dye degradation study on the BDD electrode surface demonstrated some highlights about the relationship between electrochemical oxidation process and the electrode surface morphology and boron doping level.

2. Experimental

2.1. BDD electrode preparation and characterization

Hot filament chemical vapor deposition (HFCVD) technique was used to produce electrodes formed from plate-shaped titanium (Ti) substrates recovered with BDD films. These BDD/Ti electrodes with the dimensions of 25 mm × 25 mm × 0.5 mm were prepared from H_2 (99%) and CH_4 (1%) gaseous mixture kept the constant in the main gas line. The doping control was obtained from an additional H_2 gas flux passing through a bubbler containing a solution of B_2O_3 dissolved in CH_3OH with the B/C ratio of 30,000 ppm. So, the boron was carried from the solution to the gas phase by this H_2 line where its additional flux in the reactor was controlled by a rotameter. These additional fluxes were kept at 25 and 40 sccm for E1 and E2, respectively. This means that the hydrogen responsible to carry boron from the bubbler solution was increased almost twice for E2 than that for E1, making possible much more boron addition during the E2 film growth. When B/C ratio of 30,000 ppm is used, the additional H_2 fluxes of 25 and 40 sccm to carry boron into the reactor assure the growth of heavily boron doped diamond films. Temperature and pressure inside the reactor chamber were kept at 923 K and 5.3 kPa, respectively. Both films were grown in a total deposition time of 7 h.

Top view SEM images of BDD films were obtained from a Jeol equipment JSM-5310. The quality of BDD films was analyzed from

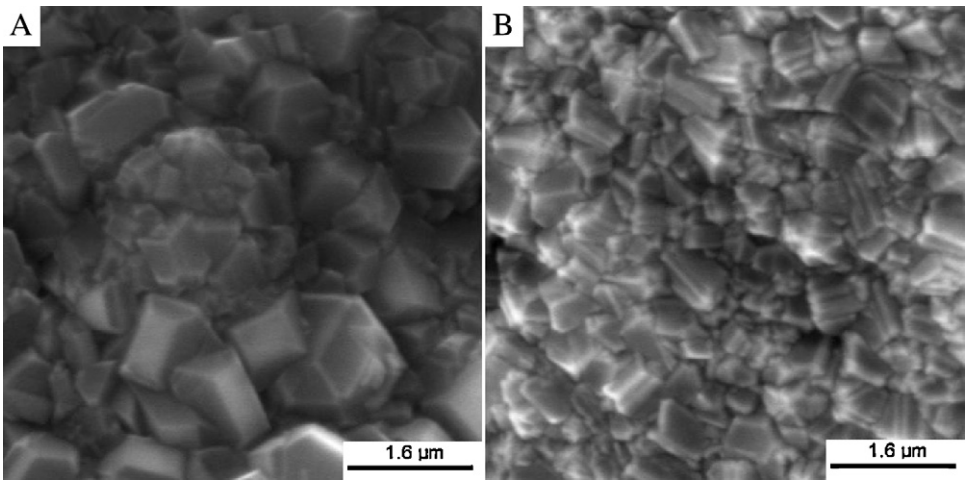

Fig. 2. Scanning electron micrographs of E1 and E2 BDD films.

Micro-Raman spectra recorded by a Renishaw microscope system 2000 in backscattering configuration. Mott–Shottky plots obtained in H_2SO_4 0.5 mol L^{-1} were used to determinate the charge carriers of the BDD/Ti electrodes.

2.2. Degradation conditions and monitoring

The electrochemical degradation of a degassed solution of the RO16 azo-dye supplied by Aldrich (~50% m/m) was performed in a polypropylene home-made single cell with capacity of 0.45 L. The BDD/Ti working electrodes (~4.15 cm^2 of the geometric area) were located at the bottom of the cell. Platinum screen, 2 cm in diameter, was used as a counter electrode and a commercial Ag/AgCl electrode (3.0 mol L^{-1} KCl solutions) as the reference electrode. All the degradation assays were performed at 20 °C and constant stirring. The solutions with 50 mg L^{-1} of the RO16 azo-dye in a K_2SO_4 0.1 mol L^{-1} (Synth) + H_2SO_4 0.1 mol L^{-1} (Synth) supporting electrolytes were electrolyzed at different current densities of 25, 50, 75, 100, 150 and 200 mA cm^{-2} and at 10, 20, 30, 45, 60, 75 and 90 min periods for each current density. These procedures were adopted for both E1 and E2 electrodes. All electrochemical measurements were carried out using a potentiostat/galvanostat AUTOLAB model PGSTAT 302 (Eco Chimie) coupled with a BRTS-10A current booster, controlled by the GPES software.

The RO16 azo-dye electrochemical degradation was monitored by: (1) UV–Visible (UV/VIS) Espectrophotometry (Varian Cary 50 Scan Espectrophotometer 300–600 nm); (2) RO16 azo-dye concentration (HPLC, Shimadzu, modelo 20 A, with UV/VIS SPD-20 detector, C_{18} (250 mm × 4.6 mm) Shimadzu ShimPack CLC-ODS® collum, methanol:water (70:30), 0.8 mL min^{-1} flux and UV/VIS detector at λ = 254 nm; and (3) total carbon organic (TOC, Shimadzu TOC-V_{CPN} analyzer).

3. Results and discussions

3.1. Morphologic and structural characterization of the BDD electrodes

3.1.1. SEM analysis

The top view SEM images of the diamond films deposited on the Ti substrates are represented in Fig. 2, which corresponds to a general view of the E1 and E2 electrode surface morphologies, respectively. These electrodes differ from each other by their morphology and boron content. The images in Fig. 2 show that the BDD films grew with a continuous and uniform surface morphology, characterized by well-shaped microcrystalline grains with sharp facets and crystallographic orientation varying between <1 1 1> and <2 0 0>. The images also present a well-facetted microcrystalline diamond surface for E1 and a significant increase in the smallest diamond grain population for E2. This behavior may be associated with the contents of boron for each electrode, because as the boron content increases the diamond grain size decreases [29].

3.1.2. Raman measurements

To investigate the composition and the quality of E1 and E2 BDD films the Raman's scattering spectra were registered and are also presented in Fig. 3. It is verified the presence of a Raman peak at around 1332 cm^{-1}, which corresponds to the vibration of a diamond first-order phonon [30]. The symmetric Lorenzian phonon observed at 1332 cm^{-1} change toward an asymmetric shape, as expected, for heavily doped films. The effect of boron doping is reflected in the spectral features. The diamond peak decreased in intensity due to the high B content in such films. Besides, the line also exhibited asymmetry Fano line shape of one phonon band at 1332 cm^{-1}. The Fano line shape may come from the quantum mechanical interference between the discrete phonon state and electronic continuum sites induced by the doping presence [31]. In addition, there is the appearance of the broad bands at ~500 and ~1220 cm^{-1}. The broad peak at ~1220 cm^{-1} feature increases with the B concentration increase. This is an indicative that the doping efficiency for electrode E2 is greater than that for electrode E1. The

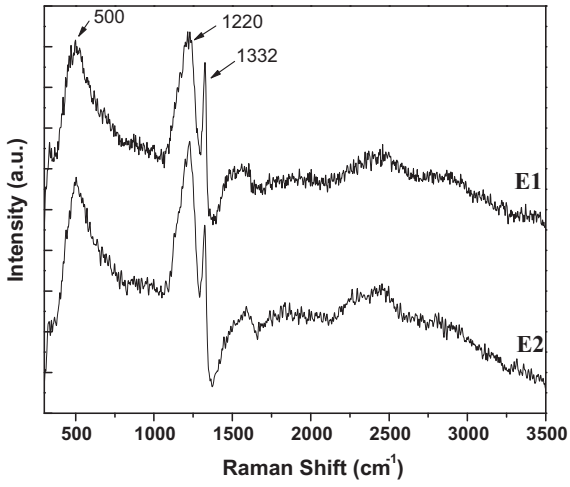

Fig. 3. Raman spectra of E1 and E2 BDD films.

boron incorporation in the lattice causes some distortion provoking defects, which cause the vibration mode at 500 cm^{-1} [32]. It is interesting to compare the boron concentration of the samples in relation of their spectrum features. For the spectra E1 and E2, the presence of G band, assigned to crystalline graphite, is evident, however it is not pronounced.

These results suggest that in both samples the amounts of non-diamond carbons are about the same. It is important to keep in mind that under our experiment conditions the desired B/C ratios were controlled by the H_2 and $B_2O_3/CH_3OH/H_2$ flows. The presence of hydrogen and oxygen during the diamond film grow affects the formation of the sp^2 carbon species. With the increase of B/C ratio the etching by hydrogen and oxygen of the sp^2-bonded graphite phase must be considered. This may explain why the G band is not pronounced. However, the presence of graphite, in the sample E2, may be hidden beneath from the other nearby band features. It is worth observing that the boron inclusion introduces lattice defects that favor the incorporation of sp^2 carbon probably at the grain boundaries. It is important to remember that the boron incorporation decreases the grain size favoring the sp^2 carbon incorporation at the diamond grain boundaries. At this point, we do not know if these features are eventually hidden in the spectrum E2 due to the strong presence of nearby band features or are due to the experimental conditions. Following the discussion above, the lack of the non-diamond carbons is not consistent with grain size presented in the electrode E2. One reasonable explanation for this is to assume that the presence of non-diamond carbons preferentially located at the grain boundaries is hidden due to the nearby band. However, such a small volume of randomly distributed non-diamond carbons may originate different conduction routes that contribute to the performance of the electrodes, especially for the electrode E2. Barnard and Sternberg [33] predicted in a theoretical study that the boron may be positioned at the grain boundaries in nanocrystalline diamond affecting the overall conductivity.

This difference on the doping level between the two electrodes was determined in terms of their charge carriers obtained from Mott–Schottky plot analyses (not shown). The acceptor concentrations were evaluated as 4.0×10^{21} and 8.0×10^{21} boron atoms cm^{-3} for E1 and E2 electrodes, respectively.

3.2. Electrochemical degradation of a simulated wastewater containing the RO16 azo-dye

At this point, we used both samples as the anode to investigate the electrochemical degradation of a simulated wastewater containing the RO16 dye as an AOP process. The oxidation was performed on both E1 and E2 electrodes. Previous works in the literature have demonstrated that BDD is a very good candidate for pollutant degradation because of their high O_2 evolution overpotential leading to a high current efficiency [34,35]. Besides, the BDD on Ti the substrate provided high electrical conductivity, electrochemical inertness and a high mechanical strength.

3.2.1. UV/VIS analysis

In order to examine the activity of the BDD electrodes, the absorbance of the RO16 solutions were investigated from UV–VIS spectra. Bulk electrolysis was studied using supporting electrolyte of 0.1 mol L^{-1} K_2SO_4 + 0.1 mol L^{-1} H_2SO_4. The current density influence was also investigated, on the degradation rates, for both E1 and E2 electrodes.

Fig. 4E1 and E2 shows the absorption spectrum of RO16 azo-dye, characterized by two bands, which can be associated to its intense orange color. The first one is located in the UV region, with their maxima located at ~390 nm, and the second one in the visible region located at ~500 nm. The absorbance band at ~500 nm is due to the n–π^* transitions of the chromophobic azo group (–N=N–) present in the RO16 molecules and that at ~390 nm are due to the π–π^* (transitions related to the aromatic rings bonded to the azo group). From the intensity of these two bands, it was possible to observe that the azo group bonds rupture and reduction of the aromaticity as the color of the solution was decreasing. For both electrodes, it is possible to observe in Fig. 4 an extreme reduction in the intensities of the two azo-dye absorbance bands as a function of the electrolysis time, since at the end of the 90 min these two bands are almost totally vanished. This states the great efficiency of the electrochemical treatment for the color reduction by using BDD/Ti electrodes. It is interesting to highlight that both electrodes were more efficient in the rupture of the azo group than that in the aromatic bonds of the azo-dye molecule. For all experiments, the highest doped electrode E2 was more efficient for both, aromaticity reduction and azo group fracture when compared to those for electrode E1.

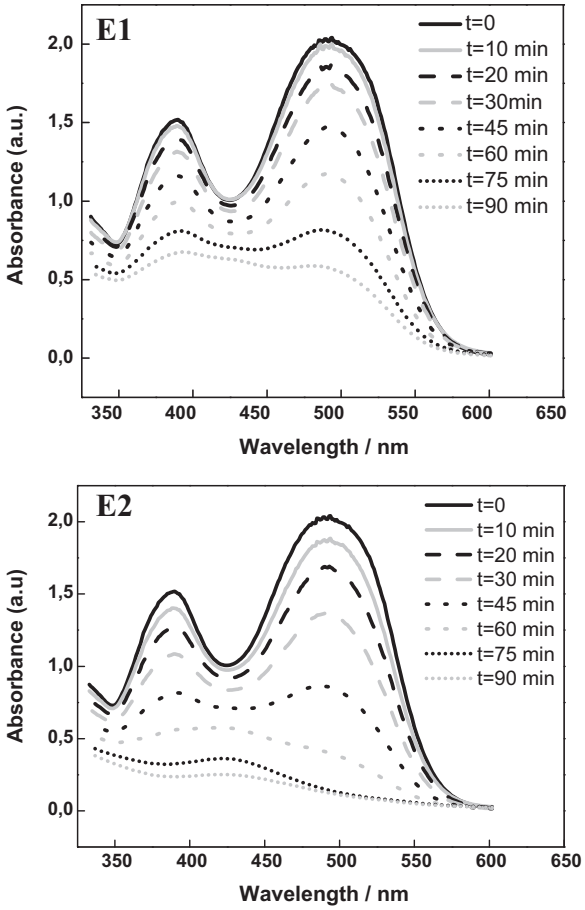

Fig. 4. UV/VIS spectral changes of the RO16 azo-dye in aqueous solutions as a function of the electrolysis time of 10, 20, 30, 45, 60, 75 and 90 min at 50 mA cm^{-2} current density using E1 and E2 electrodes.

From the Mott–Schottky plot (MS) the estimated concentrations of the charge carriers for both electrodes are in the same range of 10^{21} boron atoms cm^{-3}. However, the Raman spectra showed that the E2 presents a pronounced asymmetric Fano-like lineshape indicating a higher boron concentration than that for E1 electrode. Knowledge about the boron doping is quite limited and more studies are needed. May et al. [36] suggested that the majority of the boron concentration that does not contribute to the conductivity is at the grain boundaries and contribute to an alternative way for current flow. The spectrum E2 does not give us strong evidence related to the presence of sp^2 structure that would be responsible for the grain boundary contributions. Nonetheless, the grain size decrease

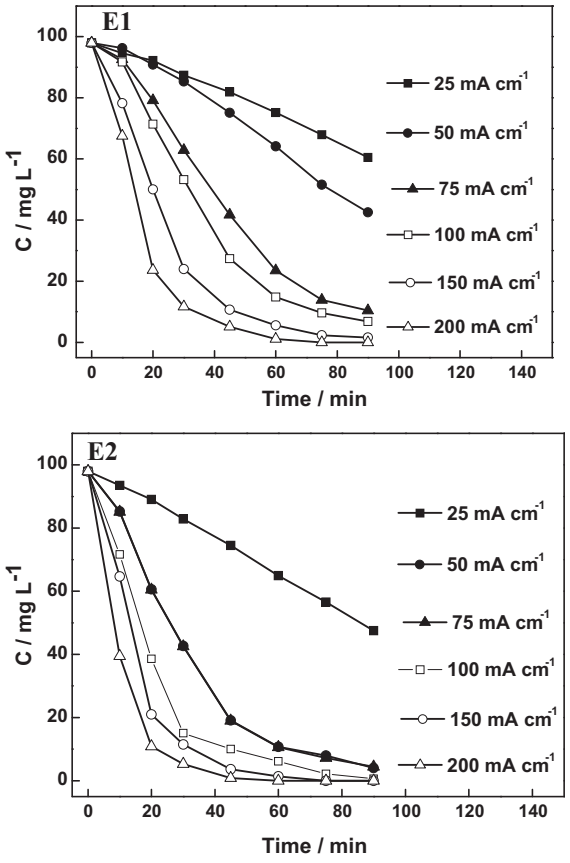

Fig. 5. Variation of the RO16 azo-dye concentration at λ = 388 nm as a function of the electrolysis time for the electrodegradation assays of 25, 50, 75, 100, 150 and 200 mA cm^{-2} using E1 and E2 electrodes.

observed for E2 electrode supports the possible sp^2 contribution coming from its highest grain boundary density. In this sense, the best results obtained for electrode E2 may be associated to a mixed conductivity at the electrode surface. It is important to point out that we did not consider the role of surface termination that may also have a strong contribution in the electrochemical response of the electrodes.

In order to understand the RO16 azo-dye degradation kinetic the variation of the RO16 azo-dye solution at λ = 388 nm absorbance region was analyzed as a function of the electrolysis time. The electrodegradation assays were performed at different current densities of 25, 50, 75, 100, 150 and 200 mA cm^{-2} by using both E1 and E2 electrodes. These results are shown in Fig. 5, where for electrode E2 the concentration values of 50 and 75 mA cm^{-2} are the same. Consequently, these curves are overlapping. The aromatic compound concentrations on the RO16 azo-dye solution decrease exponentially as a function of the electrolysis time for both electrodes studied. This behavior was observed for all current densities performed during the electrolysis assays and was progressively more pronounced as the current density was enhanced.

Considering the first 40 min of this AOP it can be seen that the E1 electrode was less efficient for electrodegradation of the RO16 azo-dye aromatics than that for E2 electrode in the whole range of current densities. For electrode E2 the concentration of the aromatics in the colorant solution was almost vanished at 200 mA cm^{-2} in the same time period. The slower decrease of the absorbance at 238 nm for the E1 electrode can be attributed to a higher rate of intermediate formations resulting from the electrodegradation of the RO16 azo-dye molecules, which still contains benzene rings. For current densities higher than 75 mA cm^{-2} the superiority in

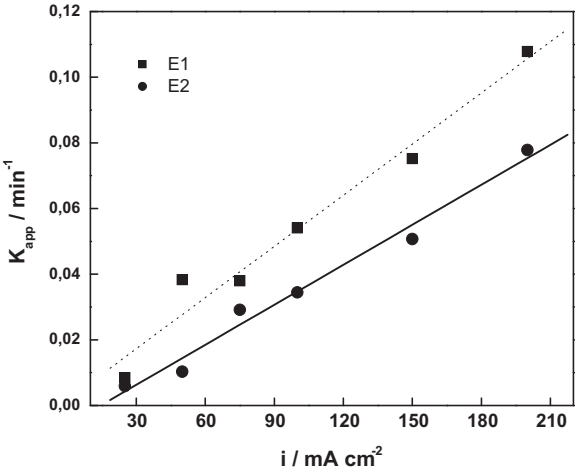

Fig. 6. Kinetic constant variation from RO16 azo-dye electrodegradation process as a function of the applied current density for E1 and E2 electrodes ([RO16]$_0$ = 50 mg L^{-1}).

the performance of E2 electrode is evident. This behavior can be linked to the higher boron concentration of the E2 electrode than that for E1 contributing to enhance the electric forces responsible for the electrogenerated •OH radicals. The main consequence is the increase in the electrochemical conductive process on the E2 surface. The exponential profile of the RO16 azo-dye absorbance curves as a function of the time point to a pseudo-first order kinetic for the reactions involved in the electrodegradation of this colorant. The apparent kinetic constant (k_{app}) can be linked to the dye concentration by Eq. (3).

$$\ln \frac{[\text{Colorant}]}{[\text{Colorant}]_0} = -k_{app}t \quad (3)$$

where [Colorant] is the concentration of the dye at time t, [Colorant]$_0$ is the initial concentration of the dye, and k_{app} is the rate constant.

The k_{app} as a function of the applied current density is presented in Fig. 6 for both BDD/Ti electrodes. A linear relationship between the kinetic constant and the current density as the k_{app} increase may be observed for E1 and E2 electrodes. This behavior evidence that the AOP process is charge transfer controlled by the electrode surface for the electrodegradation of the RO16 azo-dye molecules. Besides, the electrode E2 presented a higher average efficiency (approximately 45%), in terms of k_{app}, when compared with the electrode E1.

This highest performance for E2 electrode was traduced in terms of its efficiency for the solution discoloration. Since the highest k_{app} values was observed at 200 mA cm^{-1}, the orange color of this colorant was completely vanished after 40 min of experimental time. This high efficiency on the discoloration of the RO16 azo-dye solution can be associated to the electrochemical degradation process of the RO16 azo-dye molecules as well as other organic molecules present in the 50% RO16 chemical reagent.

3.2.2. TOC measurements

To quantify the organic load presented at the end of the AOP processes the total organic carbon (TOC) analysis was performed. TOC is an indicative of the efficiency of the electrochemical process to mineralize the organic matter present on the colorant solution. Fig. 7 presents the results of the TOC removal as a function of the applied current density for E1 and E2 electrodes. From these results, the mineralization efficiency of the organic compounds in the RO16 azo-dye solution increased as a function of the applied current density for both electrodes. The electrode E2 presented a higher

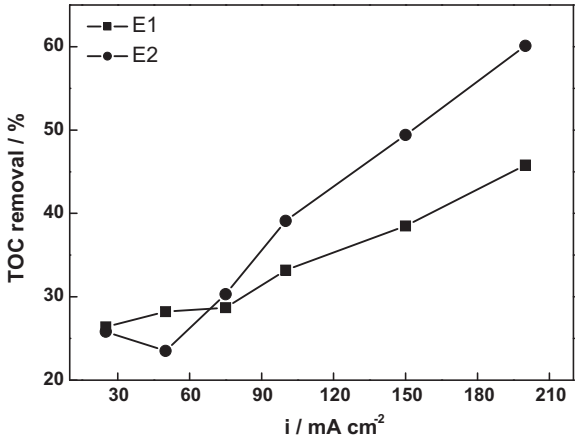

Fig. 7. TOC removal efficiency as a function of the applied current densities during the electrodegradation process using E1 and E2 electrodes.

efficiency for the TOC reduction than that for E1 electrode. The E2 electrode propitiated about 60% TOC elimination against about 40% removal for E1 electrode at the highest applied current density. The electrochemical treatment of the RO16 azo-dye solutions with BDD/Ti electrodes containing different doping levels presented a significant TOC removal, in addition to the complete color removal.

3.2.3. HPLC qualitative detection

The aromatic intermediates produced during each electrodegradation of the RO16 dye solutions were qualitatively detected by high-performance liquid chromatography (HPLC) by using the 254 nm wave length detector. The chromatographic signal at 254 nm is related to the aromatic compounds that compose the colorant solution, including the RO16 azo-dye. Fig. 8 presents the chromatograms of the RO16 azo-dye solution before the electrochemical treatment (1) and the concerning chromatograms of the solutions after the electrolytic assays at 200 mA cm^{-2} for E1 (2) and E2 (3) electrodes. The chromatogram 1 presented in Fig. 8 shows six peaks related to the aromatic compounds with different polarities and retention times, for the RO16 azo-dye solution without the electrochemical treatment. These aromatic peaks were named, in the chromatogram, from A to F. The higher intensity peaks C and E on this chromatogram are related to the RO16 azo-dye and some by-product of the colorant synthesis. They are probably responsible for the color of the solution. The less intense peaks are related with impurities of the 50% RO16 azo-dye solution. After the electrochemical treatment at 200 mA cm^{-2} with E1 and E2 electrodes (chromatograms 2 and 3) the peaks A–F are completely vanished. This is an indicative that the AOP using the BDD/Ti electrodes were efficient on the elimination of these aromatic compounds. The emerging G peak in low retention time indicates the presence of more polar aromatic compounds that present smaller aromatic chain.

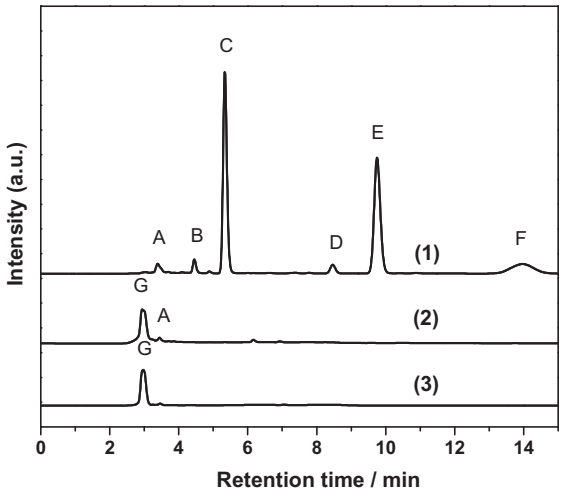

Fig. 8. Chromatograms (HPLC; λ = 254 nm) of the RO16 azo-dye solution (50%) without electrochemical treatment (1) and the colorant solutions after electrochemical treatment of (90 min at 200 mA cm^{-2}) using E1 (2) and E2 (3) electrodes.

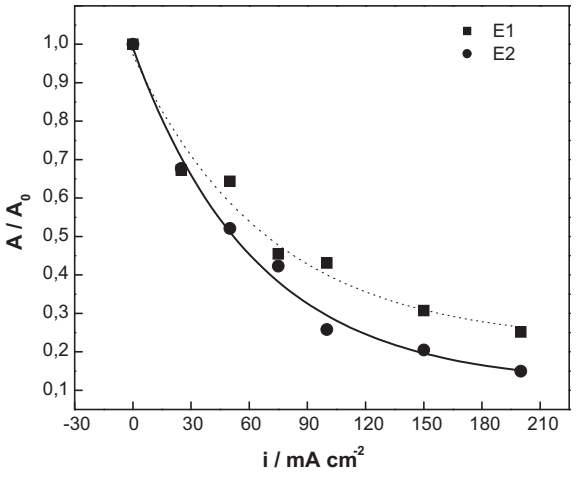

Fig. 9. Normalized total chromatographic area as a function of the applied current for electrochemical treatment of the RO16 azo-dye solution (50%) using E1 and E2 electrodes.

The variation of the normalized total chromatographic area as a function of the applied current for electrochemical treatment with E1 and E2 electrodes is presented in Fig. 9. In this case, the integration of the chromatograms obtained for the solutions after each treatment can be considered as an average of the total concentration of the aromatic compounds detected at 254 nm. The efficiency of the BDD/Ti electrodes on the electrochemical degradation of the aromatic compounds present in the colorant solution (RO16 azo-dye molecules and its synthesis products) is almost the same for current densities of 25, 50 and 75 mA cm^{-2}. Furthermore, similar behavior was observed for those compounds formed during the RO16 azo-dye solution degradation. As the applied current density increased, the E2 electrode showed a higher efficiency in the total or partial degradation of the aromatic compounds present in the RO16 azo-dye solution than that for E1 electrode. This is an evidence of the higher percentage of the aromatics reduction (∼85%) of the E2 electrode against ∼75% for the E1 electrode.

Although the non-complete TOC removal from the RO16 azo-dye solution occurred, these BDD/Ti electrodes were effective on the aromatic compound degradation. This aromatic reduction of the RO16 azo-dye solution is important in terms of the environmental point of view. This result of the sharp drop in the total concentration of aromatic compounds is indicative of the formation of compounds of aliphatic chains (Fig. 9). The aliphatic chain may be more susceptible to the microbial degradation and, probably, may be biodegradables [37]. Nevertheless, as the intermediary compounds have not been characterized, it is not possible to identify their toxicity.

4. Conclusion

The above results presented the production, characterization and application of BDD/Ti electrodes with two different doping levels in the electrochemical degradation process of the RO16 azo-dye solution. SEM and Raman measurements demonstrated the

strong influence of boron on diamond morphology as well as for its different conduction route due to the sp^2 presence at grain boundaries. This behavior may contribute to the performance of the electrodes, especially for the electrode E2, which presented the smallest grain size. Both BDD/Ti electrodes were effective on the aromatic compound degradation. They made possible the total color removal of the solution as well as the TOC reduction and the aromatic compound elimination. The highest doped E2 electrode was more efficient than the E1 electrode, mainly for current densities higher than 75 mA cm^{-2}, showing a doping level dependency of diamond electrodes with their efficiencies. The AOP showed to be a charge transfer controlled process with a pseudo first-order kinetic process.

Acknowledgments

The authors would like to thank FAPESP, CNPq and CAPES for the financial support.

References

[1] Y. Anjaneyulu, N.S. Chary, D.S.S. Raj, Decolourization of industrial effluents – available methods and emerging technologies – a review , Rev. Environ. Sci. Biotechnol. 4 (2005) 245–273.
[2] H.M. Pinheiro, E. Touraud, O. Thomas, Aromatic amines from azo dye reduction: status review with emphasis on direct UV spectrophotometric detection in textile industry wastewaters , Dyes Pigm. 61 (2004) 121–139.
[3] M. Stylidi, D.I. Kondarides, X.E. Verykios, Pathways of solar light-induced photocatalytic degradation of azo dyes in aqueous TiO_2 suspensions , Appl. Catal. B 40 (2003) 271–286.
[4] C.A. Martínez-Huitle, E. Brillas, Decontamination of wastewaters containing synthetic organic dyes by electrochemical methods: a general review , Appl. Catal. B 87 (2009) 105–145.
[5] E. Forgacs, T. Cserhati, G. Oros, Removal of synthetic dyes from wastewaters: a review , Environ. Int. 30 (2004) 953–971.
[6] T. Robinson, G. Mcmullan, R. Marchant, P. Nigam, Remediation of dyes in textile effluent: a critical review on current treatment technologies with a proposal alternative , Bioresour. Technol. 77 (2001) 247–255.
[7] A.B. Santos, F.J. Cervantes, J.B. Van Lier, A review on current technologies for decolourisation of textile wastewaters: perspectives for anaerobic biotechnology , Bioresour. Technol. 98 (2007) 2369–2385.
[8] M.C. Gutierrez, M. Crespi, A review of electrochemical treatments for colour elimination , J. Soc. Dyers Colourists 115 (1999) 342–345.
[9] M.M. Naim, Y.M. El Abd, Removal and recovery of dyestuffs from dyeing wastewaters , Sep. Purif. Methods 31 (2002) 171–228.
[10] K. Rajeshwar, J.G. Ibanez, Fundamentals and Application in Pollution Abatement , Academic Press, San Diego, CA, 1997.
[11] D. Genders, N. Weinberg (Eds.), Electrochemistry for a Cleaner Environment, The Electrosynthesis Company Inc., New York, 1992.
[12] D. Pletcher, F.C. Walsh, Industrial Electrochemistry , 2nd ed., Blackie Academic & Professional, London, 1993.
[13] D. Simonson, Electrochemistry for a cleaner environment , Chem. Soc. Rev. 26 (1997) 181–189.
[14] E. Brillas, P.L. Cabot, J. Casado, Chemical Degradation Methods for Wastes and Pollutants Environmental and Industrial Applications , M. Tarr, New York, 2003, p. 235–304.
[15] G. Chen, Electrochemical technologies in wastewater treatment , Sep. Purif. Technol. 38 (2004) 11–41.
[16] M. Panizza, G. Cerisola, Application of diamond electrodes to electrochemical processes , Electrochim. Acta 51 (2005) 191–199.
[17] C.A. Martínez-Huitle, S. Ferro, Electrochemical oxidation of organic pollutants for the wastewater treatment: direct and indirect processes , Chem. Soc. Rev. 35 (2006) 1324–1340.
[18] A. Kraft, Review doped diamond: a compact review on a new, versatile electrode material , Int. J. Electrochem. Sci. 2 (2007) 355–385.
[19] L. Miao, F. Chuanping, H. Weiwu, Z. Zhenya, S. Norio, Electrochemical degradation of phenol using electrodes of Ti/RuO_2–Pt and Ti/IrO_2–Pt , J. Hazard. Mater. 162 (2009) 455–462.
[20] O. Takashi, S. Kazuyuki, T. Kazuhisa, H. Katsuhiko, Photo-electrochemical degradation of some chlorinated organic compounds on n-TiO_2 electrode , Chemosphere 73 (2008) 1279–1283.
[21] H. Ji-Ming, K. Jian-Qing, M. Hui-Min, Z. Jin-Tao, C. Chu-Nan, Electrochemical activity, stability and degradation characteristics of IrO_2-based electrodes in aqueous solutions containing C_1 compounds , Electrochim. Acta 50 (2005) 5370–5378.
[22] M. Pera-Titus, V. García-Molina, M.A. Baños, J. Giménez, S. Esplugas, Degradation of chlorophenols by means of advanced oxidation processes: a general review , Appl. Catal. B 47 (2004) 219–256.
[23] C. Shao-An, F. Wai-Kit, Kwong-Yu, P.K. Shen, Optimizing electron spin resonance detection of hydroxyl radical in water , Chemosphere 52 (2003) 1797–1805.
[24] N.A. Braga, C.A.A. Cairo, J.T. Matsushima, M.R. Baldan, N.G. Ferreira, Diamond/porous titanium three-dimensional hybrid electrodes , J. Solid State Electrochem. 14 (2010) 313–321.
[25] M. Grattrell, D.W. Kirk, A study of electrode passivation during aqueous phenol electrolysis , J. Electrochem. Soc. 140 (1993) 903–911.
[26] M. Mitadera, N. Spataru, A. Fujishima, Electrochemical oxidation of aniline at boron-doped diamond electrodes , J. Appl. Electrochem. 34 (2004) 249–254.
[27] H.N. Dinh, P. Vanysek, V.I. Birss, The effect of film thickness and growth method on polyaniline film properties , J. Electrochem. Soc. 146 (1999) 3324–3334.
[28] C. Comninellis, A. Kapalka, S. Malato, S.A. Parsons, I. Poulios, D. Mantzavinos, Perspective advanced oxidation processes for water treatment: advances and trends for R&D , J. Chem. Technol. Biotechnol. 83 (2008) 769–776.
[29] N.G. Ferreira, L.L.G. Silva, E.J. Corat, V.J. Trava-Airoldi, Kinetics study of diamond electrodes at different levels of boron doping as a quasi-reversible systems , Diamond Relat. Mater. 11 (2002) 1523–1531.
[30] D.S. Knight, W.B. White, Characterization of diamond films by Raman spectroscopy , J. Mater. Res. 4 (1989) 385–393.
[31] J.W. Ager III, W. Walukiewicz, M. McCluskey, M.A. Plano, M.I. Landstrass, Fano interference of the Raman phonon in heavily boron doped diamond films grown by chemical vapor deposition , Appl. Phys. Lett. 66 (1995) 616–618.
[32] M. Bernard, C. Baron, A. Deneuville, About the origin of the low wave number structures of the Raman spectra of heavily boron doped diamond films , Diamond Relat. Mater. 13 (2004) 896–899.
[33] A.S. Barnard, M. Strenberg, Substitutional boron in nanodiamond, bucky-diamond, and nanocrystalline diamond grain boundaries , J. Phys. Chem. B 110 (2006) 19307–19314.
[34] G.R. Salazar-Banda, L.S. Andrade, P.A.P. Nascente, P.S. Pizani, R.C. Rocha-Filho, L.A. Avaca, On the changing electrochemical behaviour of boron-doped diamond surfaces with time after cathodic pre-treatments , Electrochim. Acta 51 (2006) 4612–4619.
[35] A.I. Del Rio, J. Molina, J. Bonastre, F. Cases, Study of the electrochemical oxidation and reduction of C.I. Reactive Orange 4 in sodium sulphate alkaline solutions , J. Hazard. Mater. 172 (2009) 187–195.
[36] P.W. May, W.J. Ludlow, M. Hannaway, P.J. Heard, J.A. Smith, K.N. Rosser, Raman and conductivity studies of boron doped microcrystalline diamond, facetted nanocrystalline diamond and cauliflower diamond films , Chem. Phys. Lett. 446 (2007) 103–108.
[37] Y. Hongwei, J. Zhanpeng, S. Shaoqi, Anaerobic biodegradability of aliphatic compounds and their quantitative structure biodegradability relationship , Sci. Total Environ. 322 (2004) 209–219.